IEEE Photonics Journal
An IEEE Photonics Society Publication

Open Access

A Demodulation Method of Spatial Domain for Low-Coherence Interferometry With High Accuracy and Adaptability

Volume 12, Number 2, April 2020

Chao Wang
Xuezhi Zhang
Junfeng Jiang
Kun Liu
Shuang Wang
Yuanyao Li
Tiegen Liu

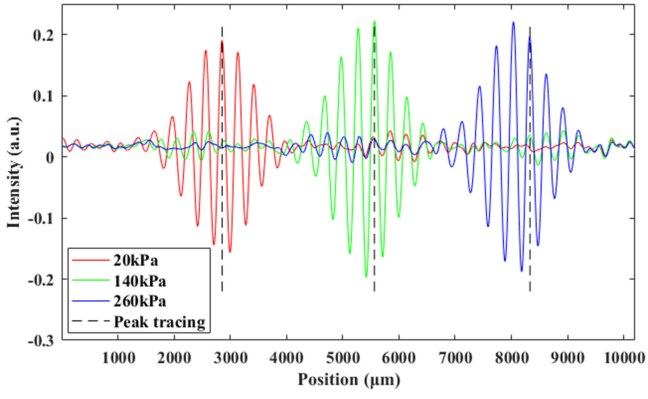

DOI: 10.1109/JPHOT.2020.2977839

IEEE photonics SOCIETY

IEEE

A Demodulation Method of Spatial Domain for Low-Coherence Interferometry With High Accuracy and Adaptability

Chao Wang [1,2,3] **Xuezhi Zhang** [1,2,3] **Junfeng Jiang** [1,2,3] **Kun Liu** [1,2,3] **Shuang Wang** [1,2,3] **Yuanyao Li** [4] **and Tiegen Liu** [1,2,3]

[1]School of Precision Instrument and Opto-Electronics Engineering, Tianjin University, Tianjin 300072, China
[2]Key Laboratory of Opto-Electronics Information Technology, Tianjin University, Ministry of Education, Tianjin 300072, China
[3]Tianjin Optical Fiber Sensing Engineering Center, Institute of Optical Fiber Sensing of Tianjin University, Tianjin 300072, China
[4]Tianjin Institute of Metrological Supervision and Testing, Tianjin 300192, China

DOI:10.1109/JPHOT.2020.2977839
This work is licensed under a Creative Commons Attribution 4.0 License. For more information, see http://creativecommons.org/licenses/by/4.0/

Manuscript received January 20, 2020; revised February 24, 2020; accepted February 28, 2020. Date of publication March 2, 2020; date of current version March 13, 2020. This work was supported in part by the National Key Research and Development Plan of China under Grant 2016YFC0401902, and in part by the National Natural Science Foundation of China under Grants U1833104, 61735011, 61675152, and 61405139. Corresponding authors: Xuezhi Zhang and Tiegen Liu (zhangxz@tju.edu.cn; tgliu@tju.edu.cn).

Abstract: A demodulation method of spatial domain based on low-coherence interferometry is proposed. The original signal of spatial domain acquired by linear CCD is filtered with all-phase filter to obtain the fringe pattern, and the phase signal of the spatial frequency domain is retained after filtering. The fringe pattern analysis is employed to avoid phase ambiguity and realize large measurement range in demodulation. Afterwards, using the centroid position of the fringe, the peak position of a single fringe pattern can be obtained, and finally the accurate peak position is calculated with seven-step phase-shifting interferometry. The demodulation method is demonstrated experimentally with Fabry-Perot sensing system. At room temperature, it is proved that the full-scale measurement error is less than 0.019% in the range of 11 kPa to 290 kPa. From −20 °C to 70 °C, the accuracy is stable and the maximum error is less than 0.054 kPa. The demodulation method has the potential to enhance the measurement accuracy and adaptability in actual environment for universal applications.

Index Terms: Optical interferometry, demodulation, fabry-perot, optical fiber sensors, pressure measurement, optical fiber applications.

1. Introduction

Due to the character of absolute distance measurement, low-coherence interferometry (LCI) is widely applied for geometric measurement [1]–[3], optical coherence tomography (OCT) [4], [5] and detection of physical quantity that can be converted to absolute distance in the field of fiber sensing [6]–[8].

Up to now, fringe pattern analysis and phase-based algorithm are two primary means of LCI demodulation. Fringe pattern analysis employed pattern position of the LCI fringe for demodulation, such as envelope [9] or peak position [10], [11]. This method requires much less computation than

phase-based algorithm, thus can achieve high-speed demodulation. However, the fringe pattern is susceptible to the distortion of the interference pattern [12], so it is hard to realize high accuracy. In 2014, Wang *et al.* [13] retrieved the peak position of zero-order fringe pattern and thus improved the precision of LCI. However, the calculation is complicated and the measurement accuracy and range are limited because the method only compensated the location-dependent birefringence dispersion. On the other hand, the phase-based algorithm employed the phase signal of frequency domain for demodulation and has higher sensitivity [14]. Since the phase period is 2π, phase ambiguity is the most significant problem to be solved. Some researchers focus on confirming the fringe order to achieve phase unwrapping. In 2012, Jiang *et al.* [15] recovered the absolute phase of spatial frequency domain (SFD) by selecting a specific wavenumber and unwrapping the overlapped phase signals. In 2015, Wang *et al.* [16] improved the accuracy of the SFD method by selecting multiple wavenumbers. However, the wavenumber and threshold for unwrapping relative phase need to be selected artificially and empirically, which limits the universality and convenience of applications. Phase-shifting interferometry (PSI) is a special phase-based algorithm, which is widely applied for surface measurement [17], [18]. Different from other methods, PSI demodulates absolute distance by calculating intensity signals corresponding to equal phase difference in spatial domain [19], and it has the unique advantage of high accuracy and simple computation. For PSI, the phase ambiguity also needs to be considered, otherwise, the measurement range has to be limited less than $\lambda/4$ dynamic-range limitation [20], [21].

To realize measurement of wide range and high accuracy simultaneously without selection of specific parameter in advance, a simple demodulation method is proposed. It is realized by tracing the peak position of a single fringe pattern, which avoids the problem of phase ambiguity. The all-phase filter [22] is introduced to eliminate background intensity and high-frequency noise of original signal in spatial domain, therefore, the LCI fringe pattern is obtained and its phase information is retained, which create possibilities for subsequent PSI. Seven-step PSI is employed to obtain the accurate peak position hence the high accuracy is realized as well as wide range. Besides, the centroid of filtered LCI fringe is employed to trace peak position of a single fringe pattern, hence no specific parameter needs to be selected in advance. Experimental verification of the method is realized with low-cost polarized LCI facility and Fabry-Perot (F-P) sensor. At room temperature, the absolute pressure error is less than 0.053 kPa in the range of 11 kPa to 290 kPa, so the full-scale (F.S.) measurement error is less than 0.019%. From -20 °C to 70 °C, the maximum pressure error is stable and less than 0.054 kPa. The demodulation method shows high accuracy and adaptability for actual environment and universal applications.

2. Theory

2.1 All-Phase Filtering in Spatial Domain

In addition to interference fringe, background intensity and high-frequency noise are unfavorable for demodulation. All-phase filter is employed to eliminate both of them for obtaining LCI fringe pattern. According to frequency sampling method, the form of N-length spatial frequency vector is

$$H = [H(0), H(1), \ldots, H(N-1)], \tag{1}$$

To acquire real-valued filter coefficients, the elements of vector should satisfy

$$H(k) = H(N-k), 0 \le k \le N-1, \tag{2}$$

The inverse discrete Fourier transform (IDFT) of the vector is

$$h(n) = \frac{1}{N}\sum_{k=0}^{N-1} H(k) \cdot e^{\frac{jnk2\pi}{N}}, 1-N \le n \le N-1, \tag{3}$$

In this paper, to filter the original signal, the vector H is designed as

$$H = \left[\underbrace{0\cdots0}_{q} \underbrace{1\cdots1}_{p} \underbrace{0\cdots0}_{N-2p-2q+1} \underbrace{1\cdots1}_{p} \underbrace{0\cdots0}_{q-1} \right], \tag{4}$$

where q is the cut-off frequency and p is the pass-band width. Combining Eqs. (3) and (4), the IDFT form of H can be expressed as

$$h(n) = \frac{1}{N} \sum_{k=q}^{p+q-1} e^{\frac{jnk2\pi}{N}} + \frac{1}{N} \sum_{k=N-p-q+1}^{N-q} e^{\frac{jnk2\pi}{N}}, -N \le n \le N-1, \tag{5}$$

Using the Euler's formula, Eq. (5) can be simplified as

$$h(n) = \frac{2}{N} \cdot \frac{\sin\frac{p\pi n}{N} \cos\frac{(2q+p-1)\pi n}{N}}{\sin\frac{\pi n}{N}}, 1-N \le n \le N-1, \tag{6}$$

Convolution window is available for improving filtering effect and weakening the Gibbs phenomenon, we employ Blackman window, which can be expressed as

$$w_{Bl}(n) = 0.42 - 0.5\cos\frac{2\pi n}{N-1} + 0.08\cos\frac{4\pi n}{N-1}, \ 0 \le n \le N-1, \tag{7}$$

The window function $w(n)$ is the convolution of $w_{Bl}(n)$ and its reversed form

$$w(n) = w_{Bl}(n) * w_{Bl}(-n), \tag{8}$$

Combing Eqs. (6) and (8), the filtering vector of spatial domain $g(n)$ can be expressed as

$$g(n) = \frac{1}{w(0)} h(n) \cdot w(n), 1-N \le n \le N-1, \tag{9}$$

where $w(0)$ is the normalization coefficient, and the length of $g(n)$ is $2N-1$. The vector $g(n)$ should be convoluted with original signal of spatial domain to realize filtering. Due to the real-valued, central symmetry and overlapping feature of $g(n)$, the amplitude and phase signals of SFD are retained after filtering. It should be noted that the filter $g(n)$ is phase-retained, hence the filtered signal of spatial domain is suitable for subsequent calculation.

2.2 Tracing Accurate Position of a Single Fringe Pattern With Centroid and PSI

In the ideal F-P sensing system, the LCI fringe pattern is stable and symmetric of different positions. So, the centroid of the fringe or its max value of the envelope can be employed for demodulation. However, the fringe pattern is influenced by some parameters in the actual system, such as production defects of the optical components, the non-perpendicular incident light, and the dispersion caused by the birefringent wedge. Thus, it is hard to realize high accuracy with the position of whole LCI fringe.

Tracing the peak position of a single fringe pattern can avoid the distortion of whole fringe pattern and realize higher accuracy. The relationship between peak position and cavity length is realized by calibration. In the process of calibration, the cavity length of F-P sensing unit should be set from minimum value L_1 to maximum value L_m. The length interval ΔL should be equal and make the displacement distance of the single peak less than the wavelength of LCI fringe λ. For convenience, using the peak position of zero-order fringe F_0 of cavity length L_1 as the initial value, its position from $pp(L_2)$ to $pp(L_m)$ can be calculated with recurrence method

$$\begin{cases} pp(L_1) = sp(F_0) \\ pp(L_i) = sp(PN), \{[sp(PN) < pp(L_{i-1})] \cap [sp(PN+1) > pp(L_{i-1})]\}, 2 \le i \le m \end{cases}, \tag{10}$$

where $pp(L_1)$ is the initial value which is the peak position of zero-order fringe of L_1 as $sp(F_0)$, $pp(L_i)$ is the subsequent peak position involved in measurement when the cavity length is L_i. The

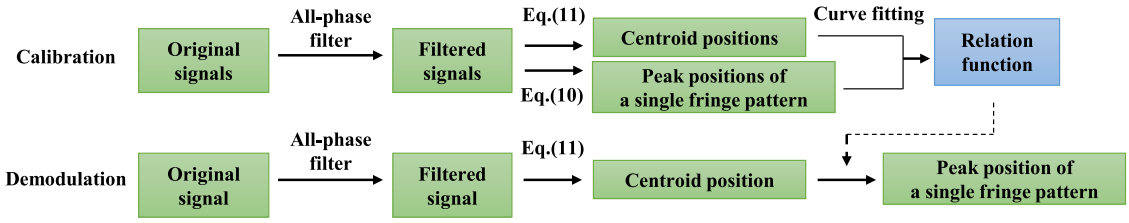

Fig. 1. Peak position of a single fringe pattern is calculated with the relation function.

maximum values of the LCI fringe is extracted as peak array, PN is the serial number of them, and $sp(PN)$ is the only peak position of single fringe pattern chosen from the peak array as it satisfies the condition of Eq. (10).

Peak position of a single fringe pattern has positive correlation property with cavity length, but it is difficult to obtain the peak position from the original or filtered signal directly on account of the distortion of the whole LCI fringe. The centroid position of the fringe pattern is suitable for calculating peak position of a single fringe pattern. The centroid position l_{cen} of the fringe pattern can be calculated with Eq. (11).

$$l_{cen} = \frac{\sum_{|I(l_p)|\geq 0.3I_{\max}} l_p \cdot |I(l_p)|}{\sum_{|I(l_p)|\geq 0.3I_{\max}} |I(l_p)|}, \tag{11}$$

where l_p is the point position of the fringe pattern, $I(l_p)$ is the intensity value of the point and $I_{\max}$ is the max value of the fringe points.

The centroid position can be employed to obtain the peak position of a single fringe pattern, because both of them move synchronously with the change of cavity length. In the calibration process, the peak position and centroid position of LCI fringe of different cavity length can be calculated with Eqs. (10) and (11), so the relation function of them can be obtained with curve fitting as shown in Fig. 1. In other words, the calculated value of peak position can be realized with centroid position, and the actual peak is the nearest one to the calculated value. The correct judgment of peak position is on condition that the absolute position error between the calculated value and actual peak is less than $\lambda/2$. In the process of demodulation, the peak position of a single fringe pattern can be calculated with the relation function, therefore no specific parameter needs to be selected in advance.

The resolution and accuracy of demodulation based on tracing peak position of a single fringe pattern is limited to the size of CCD pixel. The accuracy can be improved by employing seven-step PSI [23], [24] on condition that the step of phase difference is equal and fringe envelope is locally linear. As the LED light source has gaussian spectrum, and the sampling points of the LCI fringe pattern acquired with linear CCD are equally spaced in spatial domain, the condition can be satisfied. Therefore, the relative phase $\varphi(x)$ of a single sampling point x composing the LCI fringe pattern can be calculated as

$$\varphi(x) = \arctan \frac{3I(x-\frac{\lambda}{4}) - 3I(x+\frac{\lambda}{4}) + I(x+\frac{3\lambda}{4}) - I(x-\frac{3\lambda}{4})}{4I(x) - 2I(x-\frac{\lambda}{2}) - 2I(x+\frac{\lambda}{2})}, \tag{12}$$

where x is the position of the point, λ is the wavelength of the LCI fringe, and the sample interval of intensity is $\lambda/4$. The relative phase of the sampling point alters periodically with the interference fringe, and the wavelength λ of a single fringe pattern corresponds to a phase period of 2π. It should be noted that the value of the relative phase corresponding to the peak position of the single fringe pattern is zero. Therefore, the least square fitting can be employed for obtaining the relationship between sampling point position and relative phase, and the point of intersection between the fitted curve and horizontal axis is the accurate peak position of the single fringe pattern [13].

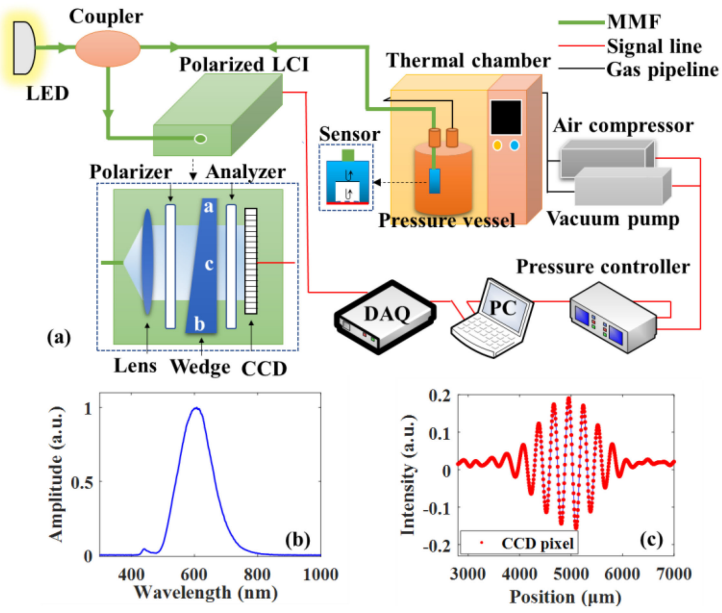

Fig. 2. (a) Schematic diagram of the experimental system. (b) The spectrum of the light source. (c) The wavelength λ of the filtered LCI fringe pattern is composed of 44 pixels.

In the process of calculating relative phase with Eq. (12), the sampling point is discarded if the denominator is equal to zero. The accurate peak position is calculated according to the sensitive phase information, so the accuracy can be improved to sub-pixel level.

3. Experimental Results

In order to verify the theoretical analysis in the second section, calibration and experiment are carried out to investigate the accuracy and adaptability of the proposed demodulation method with pressure measurement system and F-P sensor. The silicon wafer of the sensor is sensitive to pressure, and the inflection of it leads to the length change of the F-P cavity. The F-P sensor employed in this paper is the same type as Ref. 25. The thickness of the silicon wafer is 50 μm, and the Young's modulus and Poisson's ratio are 130 Gpa and 0.2782, respectively. The radius of the F-P cavity is 1.2 mm.

The schematic diagram of the low-cost demodulation section based on LCI and the experimental system is shown in Fig. 2(a). The light from LED propagates in the multimode fiber (MMF) and enters into F-P sensor via 3 dB coupler. The spectrum of the light source is shown as Fig. 2(b), and the wavelength range of the light source is from 408 nm to 908 nm. MMF is employed as lead-in and lead-out waveguide for improving the coupling intensity between optical fiber and optical devices. The reflected light from sensor is guided into the polarized LCI section, which is composed of convergent lens, polarizer, birefringent wedge, analyzer and linear CCD in sequence. The wedge can generate continuous optical path difference (OPD) induced by difference of refractive index between ordinary and extraordinary light. The wedge is made of MgF_2, the refractive index difference is 0.0118, and the angle is 8°. The side lengths a, b, c are 2.3 mm, 6.52 mm and 30 mm, respectively. When the OPD generated by the wedge is the same as twice the cavity length of F-P sensor, the LCI fringe appears on the corresponding position of CCD. The position of the fringe alters with the length change of F-P cavity, and it is realized with the variation of pressure and temperature. The ambient pressure is set from 11 kPa to 290 kPa with the accuracy of 0.02 kPa by pressure controller, and the ambient temperature is from -20 °C to 70 °C in the thermal chamber. The linear CCD has 3000 pixels, and the size of each pixel is 7 μm. The wavelength λ of a single

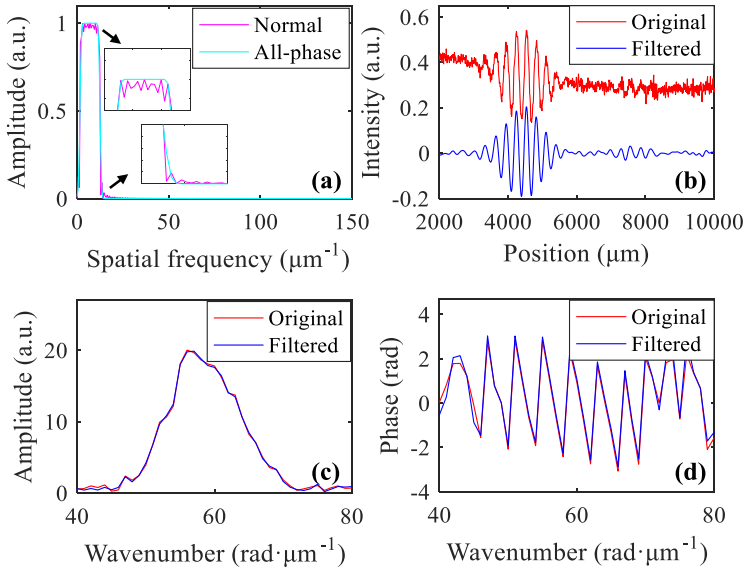

Fig. 3. (a) Response curves of normal frequency sampling filter and all-phase filter in SFD. (b) The original signal and filtered signal with all-phase filter in spatial domain. (c) Wavenumber-amplitude curves of original and filtered signal in SFD. (d) Wavenumber-phase curves of original and filtered signal in SFD.

fringe pattern is composed of 44 pixels (marked with red points) as shown in Fig. 2(c), so λ is 308 μm.

Fig. 3(a) shows the response curves of normal frequency sampling filter and all-phase filter in SFD. The parameters *N*, *p*, *q* of the filters are set to be 150, 10 and 2, respectively. The Gibbs phenomenon of the all-phase filter is eliminated and the transmission characteristics is improved compared with the curve of normal filter. Fig. 3(b) shows the original and filtered signal after all-phase filtering in spatial domain. The filtered signal makes a move of *N*-1 after filtering, and we move it back to compared it with the original signal. The relative position of each peak remains unchanged in the whole signal. The background intensity and high frequency noise of original signal are removed, nevertheless, the LCI fringe pattern is completely retained. Figs. 3(c) and 3(d) illustrate the comparison of amplitude and phase curves with discrete Fourier transform before and after all-phase filtering in SFD. It can be seen that the curves of wavenumber-amplitude and wavenumber-phase are retained after filtering. The all-phase filtering is conducive to subsequent calculation of PSI.

Fig. 4 shows the positions of the filtered LCI fringe pattern when the ambient pressure is 20 kPa, 140 kPa and 260 kPa at room temperature (25 °C). With the increase of the ambient pressure, the position of the fringe pattern gradually moves to the right. It should be noted that not only the whole fringe pattern moves, but also the relative position and amplitude of every peak. For example, in the process of moving to the right, the relative position of the zero-order fringe of 20 kPa (marked with dashed line) alters, and it even changes to be the first-order when the ambient pressure is 260 kPa as shown in Fig. 4. As a result, the pattern of the whole LCI fringe changes at different pressures, and demodulation methods based on envelope or centroid of it will lead to fairly big error. Tracing the peak position of a single fringe pattern can avoid the distortion of whole fringe pattern and realize higher accuracy.

Centroid position, which can be calculated from the filtered signal directly, is not suitable for measuring ambient pressure accurately. However, it is suitable for obtaining the peak position of a single fringe pattern according to Fig. 1. Fig. 5(a) shows the relationship between centroid position and peak position of a single fringe pattern, and Fig. 5(b) shows the absolute position error. It can be seen that the absolute error of peak position is between -34.2 μm and 32.3 μm, which is much less than $\lambda/2$ as 154 μm, so it will not result in the misjudgment of actual peak position.

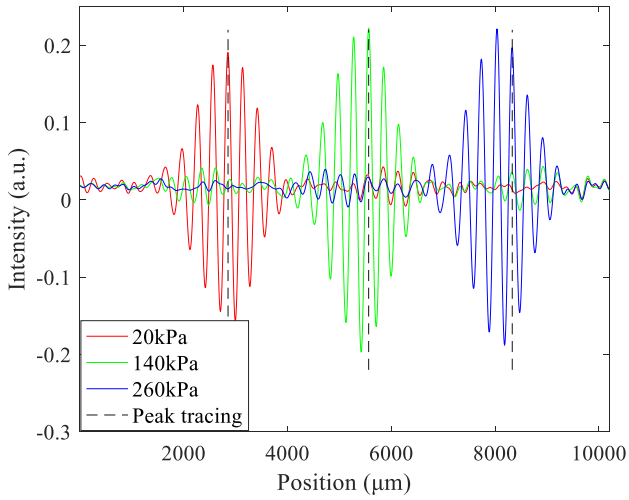

Fig. 4. The filtered LCI fringes at ambient pressure of 20 kPa, 140 kPa, 260 kPa, and the dashed line shows the position modification of a single fringe pattern.

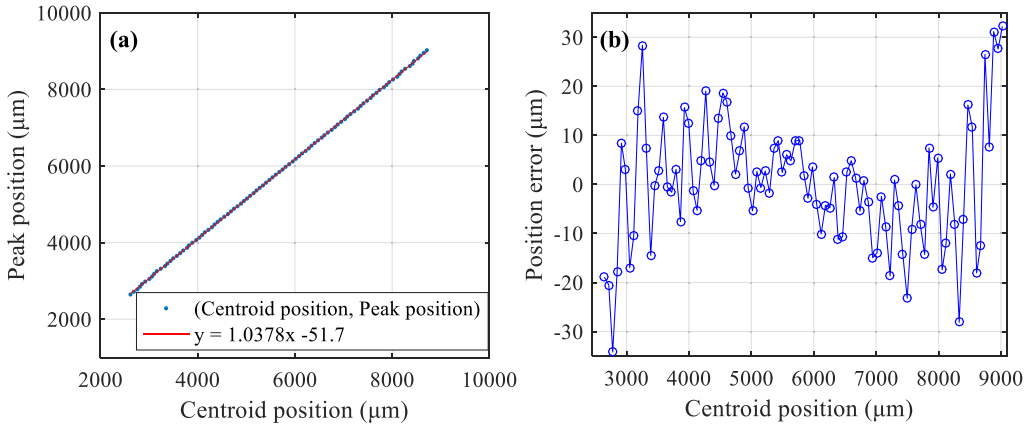

Fig. 5. (a) Relationship between centroid position and peak position of a single fringe pattern. (b) Error curve of centroid position and peak position of a single fringe pattern.

Fig. 6(a) shows the relationships of proposed method and fringe pattern position methods, such as centroid method, envelope method, and peak position method. The envelope method employs the Fourier transform to calculate the envelope position, which is the position of the maximum value of the envelope [26]. The peak position of single fringe pattern and centroid position are calculated with Eqs. (10) and (11), and the accurate position is realized with PSI as Eq. (12). It can be seen that the correlations with pressure of centroid and envelope methods are worse than other methods because both of them suffer from the distortion of the whole fringe pattern. Tracing the peak position of a single fringe pattern can reduce such effect and realize higher accuracy. It should be noted that the slope of centroid method is different from that of peak position and proposed method. The centroid position represents the movement of the whole fringe. When the whole fringe moves to the right side with the increasement of pressure, the relative position of single fringe pattern also gradually moves to right as shown in Fig. 4. Therefore, the pressure sensitivity of single fringe pattern is higher than that of centroid position. The peak position method and proposed method are based on the position change of single fringe pattern, thus the slopes of them are different from the centroid method. Fig. 6(b) shows the relationship of absolute phase method by unwrapping

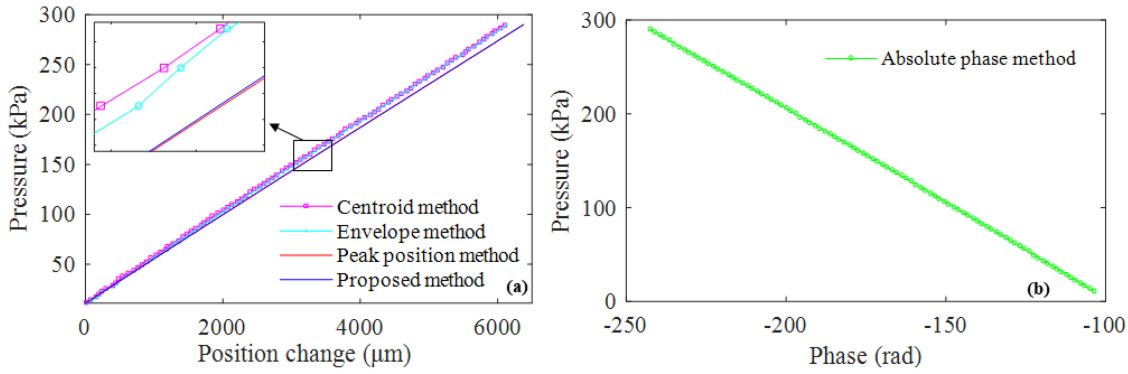

Fig. 6. (a) Relationships of centroid method, envelope method, peak position method and proposed method. (b) Relationship of absolute phase method.

TABLE 1
Measurement Accuracy of Different Methods

Methods	Absolute error range (kPa)	Relative error (F.S.)	SSE	Computational domain	Demodulation time (ms)
Centroid [10]	-1.264 ~ +1.237	0.453%	17.8995	Spatial	0.43
Envelope [26]	-1.206 ~ +1.403	0.503%	16.5280	Spatial	1.19
Peak position [11]	-0.186 ~ +0.182	0.067%	0.8028	Spatial	1.33
Absolute phase [15]	-0.122 ~ +0.104	0.044%	0.2761	Spatial frequency	2.36
Proposed method	**-0.052 ~ +0.053**	**0.019%**	**0.0507**	**Spatial**	**1.91**

relative phase [15], which is a phase-based algorithm, and it has strong correlation with ambient pressure.

The measurement errors of different methods at room temperature are shown as Table 1 and Fig. 7. Compared with other methods, the proposed method has the least error and sum of square errors (SSE), so it can be employed to measure pressure in the range of 11 kPa to 290 kPa accurately. The absolute error is reduced to 0.053 kPa, so the relative error is less than 0.019% F.S. Similar to other position based methods, all the computation of the proposed method is in spatial domain, so the computational complexity is less than that of the absolute phase method. The same set of data is demodulated with proposed method and other methods, and the average demodulation time is shown in the last column of Table 1. The software is MATLAB R2016a in the laptop with the CPU of 2.3 GHz and RAM of 8 GB. The proposed method needs more time for demodulation, it is because the computation of the proposed method is more complex than other fringe position based methods, however, the accuracy is significantly improved.

The ambient temperature is altered to investigate the adaptability of the proposed method. The ambient temperature is set to be −20 °C, 10 °C, 40 °C and 70 °C, and the pressure is from 13 kPa to 253 kPa with the pressure interval of 10 kPa. Fig. 8 and Table 2 shows the measurement error of proposed method and absolute phase method.

Compared with the absolute phase method [15], the proposed method shows higher accuracy and adaptability at different temperatures, and it should be noted that the error of proposed method keeps stable at different temperatures. For absolute phase method, the maximum error of 40 °C is 0.109 kPa, but it is enlarged to 0.181 kPa and 0.172 kPa at −20 °C and 70 °C, respectively, because the monochromatic frequency employed for unwrapping relative phase needs to be selected in advance, but the specific frequency of 40 °C is not suitable for other temperatures which will result in the increasement of error, and it is nearly impossible to choose the specific monochromatic frequency for keeping the accuracy at each temperature. Therefore, the absolute phase method is limited to the application with stable ambient temperature. In contrast, the error of

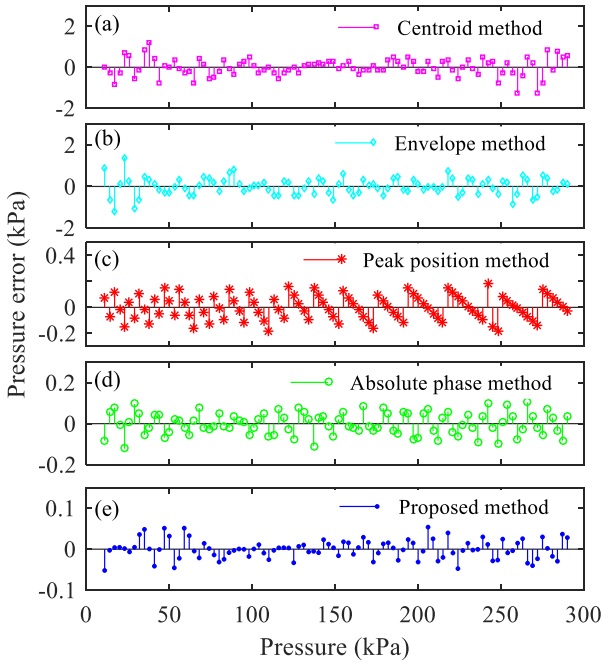

Fig. 7. Error bars of (a) centroid method, (b) envelope method, (c) peak position method, (d) absolute phase method, and (e) proposed method in the pressure range of 11 kPa to 290 kPa.

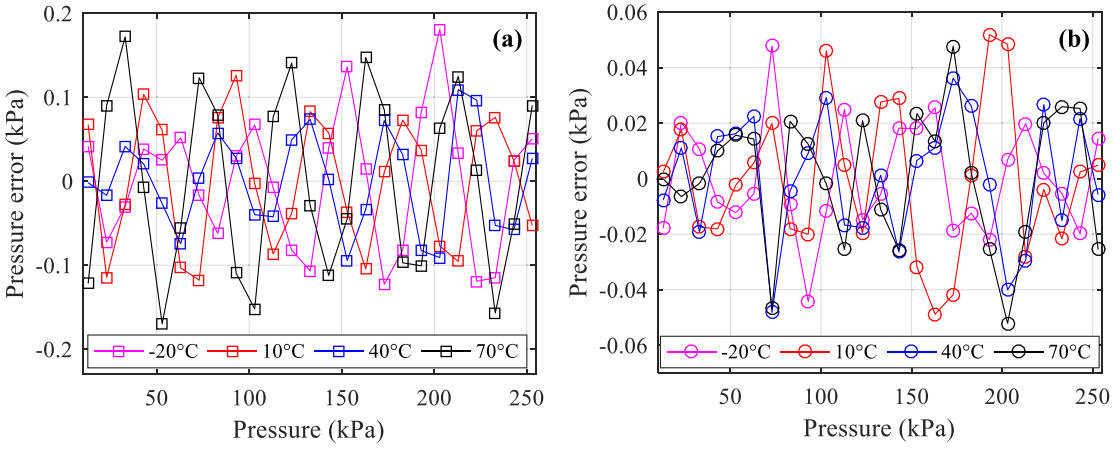

Fig. 8. Absolute pressure error of the (a) absolute phase method and (b) proposed method at different temperatures.

TABLE 2
Measurement Error of Proposed Method and Absolute Phase Method

Temperature (°C)	Absolute error (kPa)	
	Absolute phase method	Proposed method
-20	-0.123 ~ +0.181	-0.044 ~ +0.048
10	-0.118 ~ +0.126	-0.049 ~ +0.054
40	-0.094 ~ +0.109	-0.048 ~ +0.036
70	-0.170 ~ +0.172	-0.052 ~ +0.048

proposed method is nearly unchanged at different temperatures. Because the proposed method is based on calculation of fringe position in spatial domain, and no parameter need to be altered at different temperatures. The maximum pressure error is stable and less than 0.054 kPa at different temperatures. Such character of stable accuracy with temperature enable the proposed method to be applied in the external environment of varying temperatures.

Compared with fringe pattern analysis methods, such as envelope or centroid method, the proposed method realizes higher accuracy with tracing the peak position of a single fringe pattern, thus, avoid the distortion of the whole LCI fringe. After primary localization of the peak position with centroid, the accurate peak position of the single fringe is realized with PSI for demodulation, therefore, the problem of phase ambiguity is avoided. Compared with phase-based method, such as absolute phase based method, the proposed method obtains the phase signal with all phase filter and seven-step PSI, and the calculation of them is realized in spatial domain without Fourier transform, therefore, the computational complexity of the proposed method is much less than that of phase-based method, which retrieves the absolute phase of each sampling point with Fourier transform. The computation of the proposed method is more than other fringe position based method, but the accuracy is significantly improved. The higher adaptability is realized at different temperatures because no parameter needs to be selected or altered in advance. The proposed method can be employed for universal applications in actual environment.

4. Conclusions

In conclusion, we present a demodulation method of spatial domain to realize measurement of wide range and high accuracy simultaneously without selection of specific parameter in advance. The original signal of spatial domain is filtered by all-phase filter to eliminate background intensity and high-frequency noise. The centroid of the LCI fringe is employed to calculate the peak position of a single fringe pattern. PSI is employed to improve the accuracy. The demodulation method is demonstrated experimentally with a low-cost F-P sensing system. It is proven to be useful for measuring pressure with relative error less than 0.019% F.S. of room temperature. From -20 °C to 70 °C, the pressure error is stable and less than 0.054 kPa. This demodulation method is expected to play an important role in the fields of profile measurement, OCT and fiber sensing. Our further research will focus on decreasing the measurement error of the proposed method with the combination of multiple peaks chosen from the fringe pattern, thereby further improving the measurement accuracy and the adaptability.

Acknowledgment

The authors would like to thank the anonymous reviewers for their valuable suggestions.

References

[1] P. Pavlíček and G. Häusler, "White-light interferometer with dispersion: An accurate fiber-optic sensor for the measurement of distance," *Appl. Opt.* vol. 44, no. 15, pp. 2978–2983, May 2005.
[2] V. Ullmann, S. Emam, and E. Manske, "White-light interferometers with polarizing optics for length measurements with an applicable zero-point detection," *Meas. Sci. Technol.* vol. 26, no. 8, Aug. 2015, Art. no. 084010.
[3] P. de Groot, X. C. de Lega, J. Kramer, and M. Turzhitsky, "Determination of fringe order in white-light interference microscopy," *Appl. Opt.* vol. 41, no. 22, pp. 4571–4578, Aug. 2002.
[4] D. Markl, G. Hannesschläger, A. Buchsbaum, S. Sacher, J. G. Khinast, and M. Leitner, "In-line quality control of moving objects by means of spectral-domain OCT," *Opt. Lasers Eng.* vol. 59, pp. 1–10, Aug. 2014.
[5] L. Vabre, A. Dubois, and A. C. Boccara, "Thermal-light full-field optical coherence tomography," *Opt. Lett.* vol. 27, no. 7, pp. 530–532, Apr. 2002.
[6] K. Chen, Z. Yu, Z. Gong, and Q. Yu, "Lock-in white-light-interferometry-based all-optical photoacoustic spectrometer," *Opt. Lett.* vol. 43, no. 20, pp. 5038–5041, Oct. 2018.
[7] Z. Yu and A. Wang, "Fast white light interferometry demodulation algorithm for low-finesse Fabry-Perot sensors," *IEEE Photon. Technol. Lett.* vol. 27, no, 8. pp. 817–820, Apr. 2015.
[8] Y. Liu *et al.*, "Digital phase demodulation for low-coherence interferometry-based fiber-optic sensors," *Opt. Commun.* vol. 411, pp. 27–32, Mar. 2018.

[9] P. Sandoz, "Wavelet transform as a processing tool in white-light interferometry," *Opt. Lett.* vol. 22, no. 14, pp. 1065–1067, Jul. 1997.
[10] S. Chen, A. W. Palmer, K. T. V. Grattan, and B. T. Meggitt, "Digital signal-processing techniques for electronically scanned optical-fiber white-light interferometry," *Appl. Opt.* vol. 31, no. 28, pp. 6003–6010, Oct. 1992.
[11] S. Wang *et al.*, "A simple and effective demodulation method for polarized low-coherence interferometry," *IEEE Photon. Technol. Lett.* vol. 24, no. 16. pp. 1390–1392, Aug. 2012.
[12] C. Hu, X. Liu, W. Yang, W. Lu, N. Yu, and S. Chang, "Improved zero-order fringe positioning algorithms in white light interference based atomic force microscopy," *Opt. Lasers Eng.* vol. 100, pp. 71–76, Jan. 2018.
[13] S. Wang *et al.*, "Zero-fringe demodulation method based on location-dependent birefringence dispersion in polarized low-coherence interferometry," *Opt. Lett.* vol. 39, no. 7, pp. 1827–1830, Apr. 2014.
[14] L. Huang, Q. Kemao, B. Pan, and A. K. Asundi, "Comparison of fourier transform, windowed Fourier transform, and wavelet transform methods for phase extraction from a single fringe pattern in fringe projection profilometry," *Opt. Lasers Eng.* vol. 48, no. 2, pp. 141–148, Feb. 2010.
[15] J. Jiang *et al.*, "A polarized low-coherence interferometry demodulation algorithm by recovering the absolute phase of a selected monochromatic frequency," *Opt. Exp.* vol. 20, no. 16, pp. 18117–18126, Jul. 2012.
[16] S. Wang *et al.*, "Birefringence-dispersion-induced frequency domain nonlinearity compensation for polarized low-coherence interferometry demodulation," *J. Lightw. Technol.* vol. 33, no. 23, pp. 4842–4848, Dec. 2015.
[17] Q. Vo, F. Fang, X. Zhang, and H. Gao, "Surface recovery algorithm in white light interferometry based on combined white light phase shifting and fast Fourier transform algorithms," *Appl. Opt.* vol. 56, no. 29, pp. 8174–8185, Oct. 2017.
[18] T. Guo, F. Li, J. Chen, X. Fu, and X. Hu, "Multi-wavelength phase-shifting interferometry for micro-structures measurement based on color image processing in white light interference," *Opt. Lasers Eng.* vol. 82, pp. 41–47, Jul. 2016.
[19] Y. Y. Cheng and J. C. Wyant, "Phase shifter calibration in phase-shifting interferometry," *Appl. Opt.* vol. 24, no. 18, pp. 3049–3052, 1985.
[20] S. K. Debnath and M. P. Kothiyal, "Improved optical profiling using the spectral phase in spectrally resolved white-light interferometry," *Appl. Opt.* vol. 45, no. 27, pp. 6965–6972, Sep. 2006.
[21] A. Harasaki, J. Schmit, and J. C. Wyant, "Improved vertical-scanning interferometry," *Appl. Opt.* vol. 39, no. 13, pp. 2107–2115, May. 2000.
[22] X. Huang, Y. Wang, K. Liu, T. Liu, C. Ma, and M. Tian, "High-efficiency endpoint detection in optical fiber perimeter security," *J. Lightw. Technol.* vol. 34, no. 21, pp. 5049–5055, Nov. 2016.
[23] K. G. Larkin, "Efficient nonlinear algorithm for envelope detection in white light interferometry," *J. Opt. Soc. Am. A* vol. 13, no. 4, pp. 832–843, Apr. 1996.
[24] P. Sandoz, "An algorithm for profilometry by white-light phase-shifting interferometry," *J. Mod. Opt.* vol. 43, no. 8, pp. 1545–1554, 1996.
[25] C. Wang *et al.*, "Fiber optical temperature compensated anemometer based on dual fabry-perot sensors with sealed cavity," *Opt. Exp.* vol. 27, no. 13, pp. 18157–18168, Jun. 2019.
[26] G. S. Kino and S. S. C. Chim, "Mirau correlation microscope," *Appl. Opt.* vol. 29, no. 26, pp. 3775–3783, Sep. 1990.